https://doi.org/10.3311/PPch.11789

Periodica Polytechnica Chemical Engineering, 63(1), pp. 85–95, 2019

Synthesis and Characterisation of Mesoporous TiO_2 Nanoparticles by Novel Surfactant Assisted Sol-gel Method for the Degradation of Organic Compounds

Harish Phattepur[1], Gowrishankar Bychapur Siddaiah[2*], Nagaraju Ganganagappa[3]

[1] Department of Chemical Engineering, Siddaganga Institute of Technology, (Affiliated to VTU, Belagavi) Tumakuru – 572 103, India
[2] Department of Biotechnology, Siddaganga Institute of Technology, (Affiliated to VTU, Belagavi) Tumakuru – 572 103, India
[3] Department of Chemistry, Siddaganga Institute of Technology, (Affiliated to VTU, Belagavi) Tumakuru – 572 103, India
* Corresponding author, email: bsgowri@sit.ac.in

Received: 08 December 2017, Accepted: 02 April 2018, Published online: 18 May 2018

Abstract

A sol-gel method was employed to synthesise pure titanium dioxide (TiO_2) and surfactant assisted TiO_2 nanoparticles (NPs). The effect of novel surfactant viz., Lauryl lactyl lactate on photocatalytic properties of TiO_2 was studied. TiO_2 NPs were characterized by X-ray diffraction (XRD), Fourier transform infrared spectroscopy (FT-IR), UV-Vis Diffuse Reflectance spectra (DRS), Field emission scanning electron microscopy (FE-SEM), Transmission electron microscopy (TEM), Thermo gravimetric analysis (TGA), and Brunauer – Emmet - Teller (BET) surface area. Anatase phase of TiO_2 was confirmed by X-Ray diffraction pattern and the crystallite size was between 9–19 nm. Addition of surfactant improved the BET surface area, surface defects, while the agglomeration of particles was reduced. DRS results revealed that the addition of surfactant to TiO_2 sol induced a red shift of the absorption edge which resulted in the reduction of band gap from 3.23 to 3.21 eV. These physicochemical properties of TiO_2 NPs were correlated with photocatalytic degradation of phenol. About 92% of phenol degradation was observed for surfactant assisted TiO_2 NPs (SA-TiO_2). Salicylic acid and caffeine were also degraded using SA-TiO_2 NPs.

Keywords

titanium dioxide nanoparticles, Photocatalysis, phenol, sol-gel, Lauryl lactyl lactate

1 Introduction

A major environmental problem is the waste water containing undesirable organic pollutants that are released to the aquatic system. Among various methods available to remove the organic pollutants from aquatic system, photocatalytic technique is one of the most advanced oxidation method [1]. TiO_2 is one of the most studied photocatalytic material in this field [2]. TiO_2 exists in three different crystalline forms. Among them, anatase and rutile phases find many applications. A higher photocatalytic activity has been proved by anatase phase in degradation of organic compounds. TiO_2 NPs can be synthesised by various methods like sol-gel, hydrothermal, emulsion, anodization, vapour deposition, sonication, and microwave [3–10]. Reddy et al. reported the synthesis of TiO_2 NPs by molten salt method [11–14]. Zhu et al. prepared rice grain shaped TiO_2 NPs by electro spinning [15]. Cherian et al. fabricated (N, F) co doped TiO_2 NPs by pyroammonolysis of TiF_3 [16]. The properties of TiO_2 NPs depend on various factors such as the method of synthesis, the experimental conditions and the polymorph structure [17, 18]. Li and Wang synthesised TiO_2 NPs by micro emulsion method and the particle size was 10 to 20 nm. This method is too expensive, as only a small quantity of TiO_2 NPs can be obtained by using a large quantity of surfactant and oil [19]. The sol-gel is the most extensively used method for the synthesis of TiO_2, because it can be carried out at room temperature and cost effective [20]. The advantages of molten salt method are high diffusivity due to the molten reactants and do not require mechanical mixing [11]. Crystal structure, particle size, and surface porosity of TiO_2 are important factors for photocatalytic activity. However, TiO_2 has large band gap (3.2 eV) and high recombination rate of charge carriers, various modification methods are adopted to improve its activity by reducing the rate of recombination of charge carriers [21, 22]. The recombination of photo generated electron-hole pairs can be retarded by

Cite this article as: Phattepur, H., Bychapur Siddaiah, G., Ganganagappa, N. "Synthesis and Characterisation of Mesoporous TiO_2 Nanoparticles by Novel Surfactant Assisted Sol-gel Method for the Degradation of Organic Compounds", Periodica Polytechnica Chemical Engineering, 63(1), pp. 85–95, 2019. https://doi.org/10.3311/PPch.11789

doping with metal or non-metal. The charge carrier's lifetime can be extended and therefore photocatalytic activity of the material is enhanced [23–25].

The advanced materials chemistry goal is to synthesise TiO_2 nanocrystals with required shape, which results in potential materials with shape dependent properties. Crystal surface energy is responsible for crystal growth rate. The surface energy of the crystals can be enhanced or reduced by surfactant adhesion which results in anisotropic nanocrystal growth [26]. In this article, we have reported the novel surfactant viz., Lauryl lactyl lactate assisted sol-gel method for the synthesis of TiO_2 NPs and examined its photocatalytic activity for the degradation of phenol, salicylic acid and caffeine.

Phenol and its derivatives are major water pollutants in chemical industries viz., textile, petrochemical, paint and are carcinogenic and mutagenic, poses a risk to mammalian and aquatic life [27]. When waste water containing phenol is chlorinated, polychlorinated phenols are formed, which are toxic in nature. Such waste water must be treated and then released to the environment. Various parameters like catalyst dosage (0.25 to 1.5 g/L) and phenol concentration (0.1 to 0.43 mmol/L) have been examined to know the effect of photocatalytic degradation.

Wastewater coming from industries like cosmetic, paper mill, human and veterinary drugs contains salicylic acid, which is a hazardous substance. The higher concentration of salicylic acid in water leads to lung and kidney damage in human beings. Advanced treatment technologies are needed to remove salicylic acid from waste / industrial water [28].

Pharmaceutical drugs are used to treat diseases in human beings and animals and keep healthy. However, the active pharmaceutical ingredients in these medicines can enter the environment either as drug or as its metabolites [29]. High dosage of caffeine can cause nervousness and insomnia. Hence, there is a requirement of processes which can remove such ingredients from the environment. Caffeine is one such pharmaceutical ingredient. Chuang et al. synthesised TiO_2 NPs by modified homogeneous precipitation process and employed it for the degradation of caffeine [30]. Arfanis et al. prepared TiO_2 nanotubes by one step electrochemical anodization technique for the degradation of salicylic acid and caffeine [31]. In this research, an attempt has been made to degrade the pollutants in particular various concentrations of phenol. Also salicylic acid and caffeine were considered for the degradation studies.

To the best of our knowledge, no research work has been reported on synthesis of TiO_2 NPs assisted by lauryl lactyl lactate (Koplactylate) surfactant and used for the photocatalytic degradation of phenol, salicylic acid and caffeine.

2 Materials and method

2.1 Chemicals

Titanium (IV) butoxide (Ti $(OC_4H_9)_4$, 97%) was obtained from Sigma-Aldrich. Ethyl alcohol and Hydrochloric acid were procured from S. D. Fine chemicals. Salicylic acid and caffeine were obtained from Merck. Lauryl lactyl lactate ($C_{18}H_{34}O_5$) was procured from Kumar organic products Pvt. Ltd., Bangalore. Coumarin (99%) was obtained from Loba Chemie. All the chemical reagents were used without further purification. Double distilled water was used for all the experiments.

2.2 Synthesis of TiO_2 NPs by sol-gel method

SA- TiO_2 nanostructured photocatalysts were prepared by modified sol–gel method using titanium (IV) butoxide ($Ti(OC_4H_9)_4$,) as precursor. Two solutions A and B were prepared as follows. The solution A was composed of 4 mL ethanol and 0.9 mL distilled water. The solution B was composed of known quantity of lauryl lactyl lactate (0.25 mL, 0.5 mL, 0.75 mL and 1 mL), 8 mL ethanol, 2 mL titanium butoxide and 0.1 mL concentrated hydrochloric acid. Compared to other toxic additives (i.e.~~(,)~~ ammonium salts with long chain), lauryl lactyl lactate is biodegradable, inexpensive and also can control large inorganic clusters.

The solutions A and B were mixed together and stirred for about 8 min until the gel formed. After 12 h aging at room temperature, the gel was dried at 80 °C in hot air oven for 3 h. The solid was ground and subjected to calcination using muffle furnace from room temperature to 475 °C with a heating rate of 5 °C / min and the same temperature was maintained for 3 h. The TiO_2 NPs were cooled naturally to room temperature. The SA-TiO_2 NPs were marked as R [molar ratio of surfactant to titanium butoxide] equal to 0.125, 0.25, and 0.375 and 0.5. Pure TiO_2 NPs were prepared using the same method in absence of surfactant [32].

2.3 Characterisation

XRD studies of the TiO_2 materials were performed using Rigaku Smart Lab with Cu Kα radiation. Bond stretching frequencies of TiO_2 were analysed by FTIR (Bruker-alpha). Diffusion Reflectance Spectra (DRS) of TiO_2 samples were analysed using a Varian Cary 5 UV–Vis–NIR spectroscope

fitted with a 11 cm diameter integrating sphere coated with poly tetra fluoro ethylene. The surface morphologies of the prepared TiO_2 samples were obtained using Field emission scanning electron microscopy (GEMINI-ULTRA 55). The shape and size of the TiO_2 crystallites were determined using Transmission electron microscope (PHILIPS CM 2000). Thermal analysis of the as prepared TiO_2 sample was carried out using PERKIN ELMER, USA thermal analyzer. The specific surface area of TiO_2 samples were measured by Brunauer–Emmett–Teller analysis (Quantachrome NOVA-1000, USA) using N_2 adsorption–desorption isotherms at 77 K. The UV absorbance of the pollutants was measured using UV-Visible spectrophotometer (Agilent technology-Cary-60). Photoluminescence studies were recorded using fluorescence spectrophotometer (Agilent technology-Cary Eclipse).

2.4 Photo-reactor set up

The photo-reactor was procured from "HEBER" scientific, Chennai. The photocatalytic reactor consists of a medium pressure mercury vapour lamp (125 W, λmax = 365 nm) in a jacketed quartz tube. The heat generated from the lamp was removed by continuous circulation of cold water through the jacket. A set of 100 mL quartz tubes of 2.3 cm i.d., 2.7 cm o.d., and 37 cm length containing pollutant were placed surrounding the lamp. The distance between the mercury lamp and the quartz tube containing pollutant was 6 cm. The uniform distribution of catalyst particles throughout the solution was achieved using an air pump.

2.5 Degradation of pollutants

100 mL phenol of known concentration was taken in a quartz tube. To this, known quantity of catalyst was added. The quartz tube was kept in the dark for 30 min to attain adsorption-desorption equilibrium. Then, the UV light was switched on. 2 mL of aliquots were withdrawn for every 30 min interval. The samples were centrifuged at 10000 rpm using micro centrifuge (Torson, spinwin) for 10 min in order to separate TiO_2 NPs. The concentration of phenol was measured quantitatively using UV-Vis spectrophotometer at 270 nm. Spectrophotometric measurements were carried out using a quartz cell having a path length of 1 cm. Degradation efficiency was calculated using Eq. (1).

$$DE = \left(Ao - At\right) / Ao \times 100 \tag{1}$$

where, A_o and A_t are the absorbance at time zero and time t, respectively. Salicylic acid and caffeine were also analysed by the same method.

The hydroxyl radicals play a major role in the degradation of pollutants. The formation of hydroxyl radicals was detected by photoluminescence spectrophotometer using coumarin as probe molecule.

3 Results and discussion

3.1 X-Ray Diffraction patterns

Fig. 1 shows the XRD patterns of TiO_2 and SA-TiO_2 NPs calcined at 475 °C. XRD patterns confirm that all the TiO_2 NPs were in anatase phase (Peaks at 2θ = 25.25°, 37.78°, 48.32°, 54°, 55° and 62.7°) with a typical anisotropic growth along (001) direction. XRD pattern well matches with the JCPDS number 21-1272. Lattice parameters of SA-TiO_2 (R = 0.25) NPs were found to be a, b = 3.786 Å, c = 9.502 Å (Space group: I 41/a m d). XRD patterns confirm that all the TiO_2 NPs were crystalline. The calcination temperature determines the phase formation of NPs [33]. Debye-Scherrer's equation was used to estimate the mean crystallite size of TiO_2 NPs.

$$D = \left(0.89\lambda\right) / \left(\beta \cos\theta\right) \tag{2}$$

where, D is average crystallite size (nm), λ is wavelength of Cu Kα (0.154 nm), β is full width at half maximum (FWHM) in radian and θ is Bragg angle. The calculated crystallite sizes are given in Table 1. The crystallite size was varying between 9 to 19 nm. The average crystallite size of SA-TiO_2 (R = 0.25) NPs after refinement was found to be 11 nm.

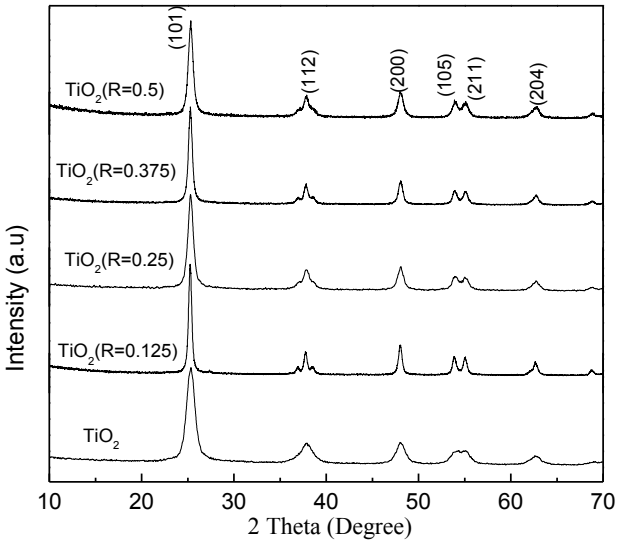

Fig. 1 XRD pattern of TiO_2 and SA-TiO_2 NPs

Table 1 XRD and BET results of TiO_2 and SA-TiO_2 NPs

Sample	Crystallite size, nm	BET specific surface area, m^2/g	Average pore size, nm	Pore volume, cm^3/g
TiO_2	11	22.34	9.7	0.081
TiO_2 (R = 0.125)	19	22.59	8.2	0.079
TiO_2 (R = 0.25)	9	40.10	8.3	0.112
TiO_2 (R = 0.375)	17	17.19	8.2	0.062

3.2 Fourier Transform Infrared Spectroscopy

Fig. 2 (a)-(c) shows the FTIR spectra of TiO_2 and SA-TiO_2 NPs. The stretching at 480 cm^{-1} corresponds to Ti-O bond. Fig. 2 (b) represents the SA-TiO_2 NPs (R = 0.25) dried at 80 °C and Fig. 2 (c) represents the SA-TiO_2 NPs (R = 0.25) calcined at 475 °C for 3 h. A comparison between these two spectra shows that organic functional groups present in surfactant (peaks between 1000 and 1600 cm^{-1}) were decomposed completely after calcination. Fig. 2 (a) represents TiO_2 NPs calcined at 475 °C for 3 h. A comparison between SA-TiO_2 (R = 0.25) with pure TiO_2 NPs after calcination suggests that there were no organic molecules associated with SA-TiO_2 NPs (R = 0.25) after calcination at 475 °C. The stretching peaks at 3400 cm^{-1} and 1630 cm^{-1} are characteristic of O-H bending of adsorbed water.

3.3 UV–Vis diffuse reflectance spectra

The UV–Vis diffuse reflectance spectra of TiO_2 and SA-TiO_2 NPs are shown in Fig. 3 (a). A red shift of SA-TiO_2 NPs was observed compared to pure TiO_2 NPs. The SA-TiO_2 NPs absorbed UV light around 396 nm, while the pure TiO_2 NPs absorbed the UV light with a lower wavelength (391 nm). The red shift of SA-TiO_2 NPs could be due to the large surface defects on particle surfaces [34]. The band gap energy was determined using Kubelka - Munk model [35].

$$F\left(R\infty\right) = \left(\left(1 - R\infty \wedge 2\right)\right) / \left(2R\infty\right) \quad (3)$$

where $R_\infty = R_{sample} / R_{reference}$, R_{sample} and $R_{reference}$ are reflectance corresponding to sample and $BaSO_4$ respectively. The plots of modified Kubelka-Munk function against band energy are shown in Fig. 3(b). The indirect band gap energies of synthesised TiO_2 and SA-TiO_2 (R = 0.25) NPs are 2.97 and 2.93 eV respectively. The band gap energies were much lower than the actual (3.2 eV). Hence, the direct band gap energies are estimated and found to be 3.23 and 3.21 eV respectively.

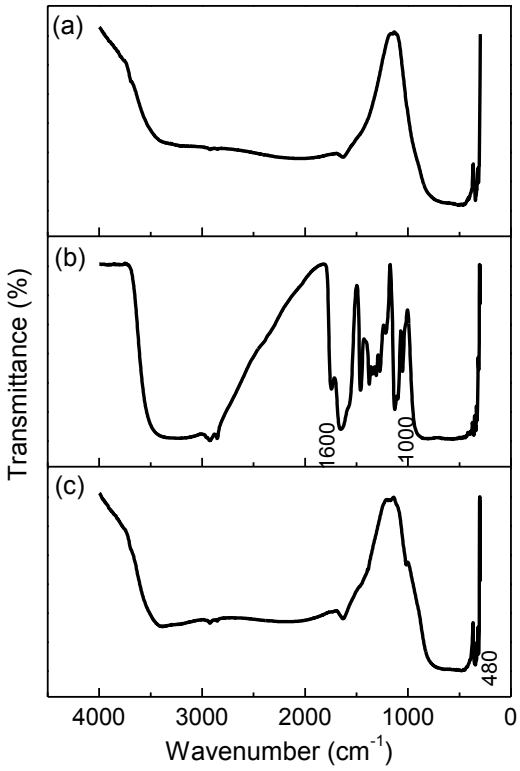

Fig. 2 FTIR spectra of (a) TiO_2 (b) As prepared SA-TiO_2 NPs (R = 0.25) and (c) Calcined SA-TiO_2 NPs (R = 0.25)

3.4 Field Emission Scanning Electron Microscopy

The information about the distribution of NPs was obtained by referring to FESEM images. The images show that the TiO_2 NPs (Fig. 4 (a), (b)) were agglomerated and formed large particle blocks, whereas the SA-TiO_2 NPs (Fig. 4 (c)-(f)) showed a lower degree of agglomeration. The addition of surfactant reduced the degree of agglomeration.

3.5 TEM and SAED analysis

Fig. 5 (a)-(d) shows the TEM images of TiO_2 and SA-TiO_2 (R = 0.25) NPs. The average size of TiO_2 and SA-TiO_2 NPs were found to be 25-30 nm and were irregular in shape. The Debye rings are from by diffraction points corresponding to the different orientations of a family of crystalline planes. SAED pattern indicates the presence of (101), (112), (200) and (204) planes in both TiO_2 and SA-TiO_2 NPs (Fig. 5 (e), (f)), are in consistent with the XRD results.

3.6 Thermo Gravimetric Analysis (TGA)

TGA analysis of TiO_2 and SA-TiO_2 (R = 0.25) NPs dried at 80 °C is shown in Fig. 6. For TiO_2 NPs (Fig. 6 a), an initial weight loss of 34 % was observed when the temperature was increased to 250 °C, which was attributed to the loss of

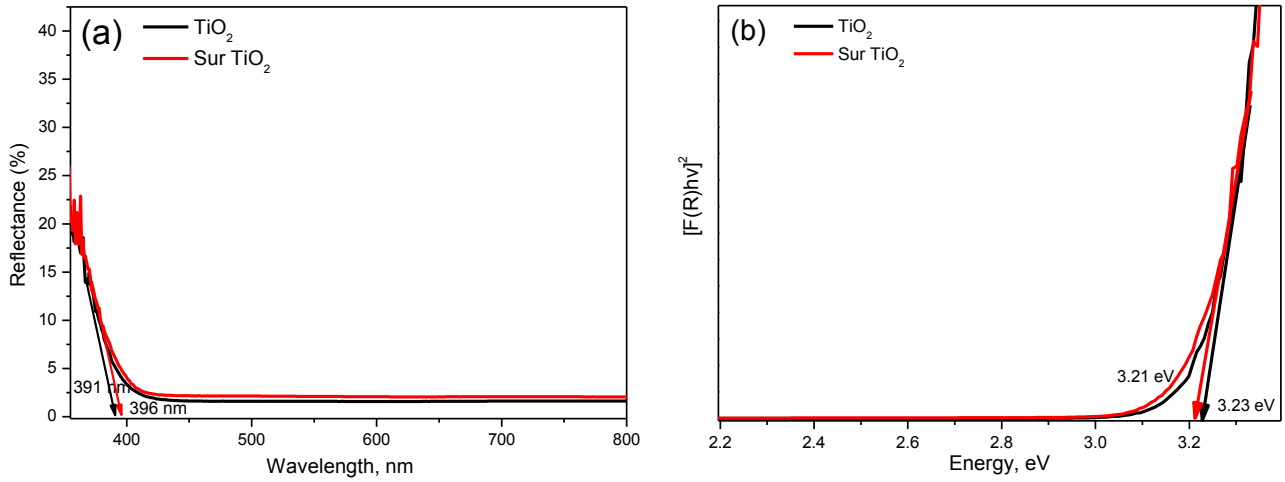

Fig. 3 (a) Diffuse reflectance spectra and (b) band gap energy of TiO_2 and SA-TiO_2 NPs (R = 0.25)

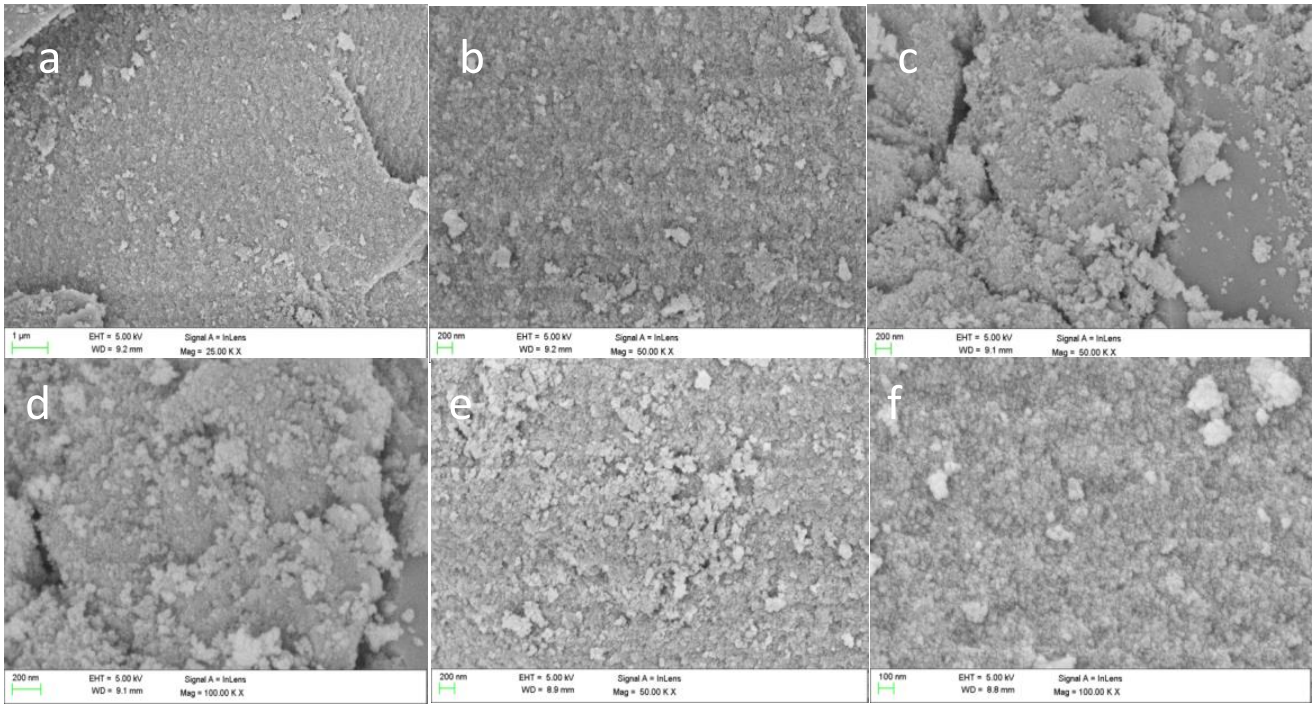

Fig. 4 FESEM images of (a, b) TiO_2 and (c-f) SA-TiO_2 NPs (R = 0.125, 0.25, 0.375 and 0.5)

physically absorbed water, ethanol and hydrochloric acid. For SA-TiO_2 NPs (R = 0.25), a further weight loss (14 %) was observed from 250 to 370 °C, which is attributed to the loss of surfactant. There after no further significant thermal effects were detected even up to 800 °C, shows the stability of the materials at higher temperatures.

3.7 BET analysis

N_2 adsorption-desorption isotherms of TiO_2 and SA-TiO_2 NPs (R = 0.125, 0.25 and 0.375) are shown in Fig. 7 (a)-(d). The pore size distribution plots are shown as inset in respective isotherms. All the 4 catalysts [TiO_2, TiO_2 (R = 0.125), TiO_2 (R = 0.25) and TiO_2 (R = 0.375)] exhibited type IV adsorption-desorption isotherms with an elongated S-type hysteresis loop for each. The higher specific surface area (40.10 m^2/g) and pore volume (0.112 cm^3/g) were observed for TiO_2 NPs with R = 0.25 when compared to other TiO_2 NPs (Pure, R = 0.125, 0.375) prepared using different quantity (0, 0.25 and 0.75 mL) of surfactant. The addition of surfactant resulted in increase of specific

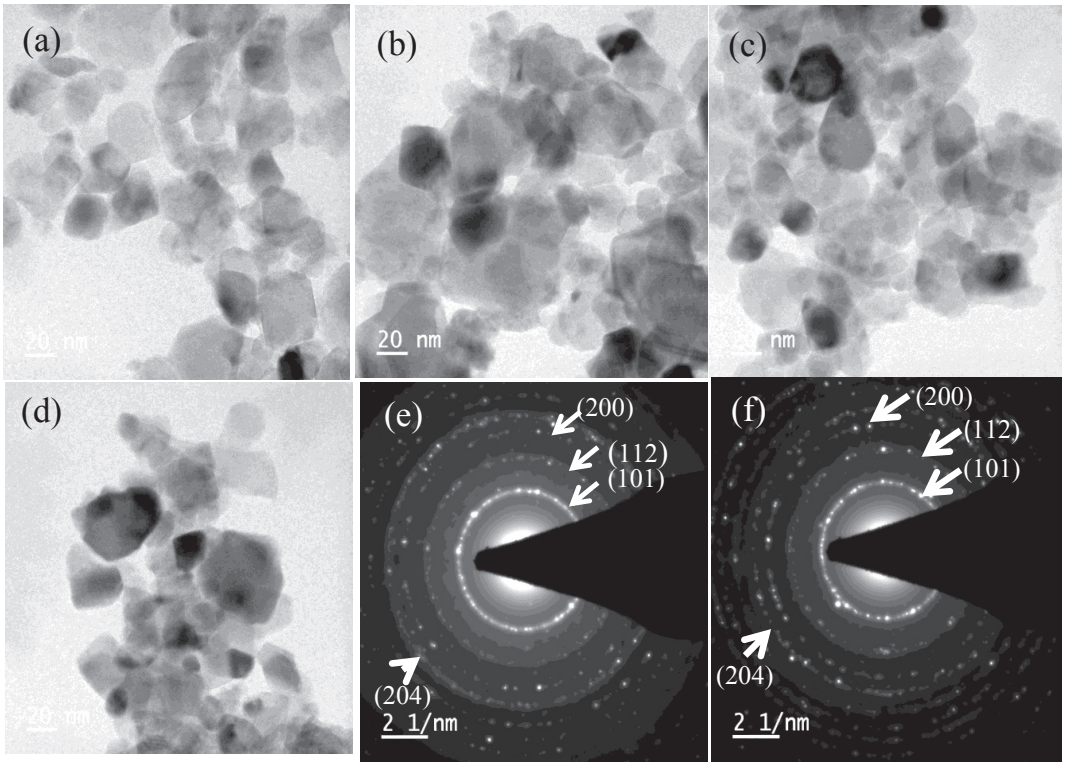

Fig. 5 TEM images of (a, b) TiO_2 and (c, d) SA-TiO_2 (R = 0.25) and SAED images of TiO_2 and SA-TiO_2 NPs (R = 0.25)

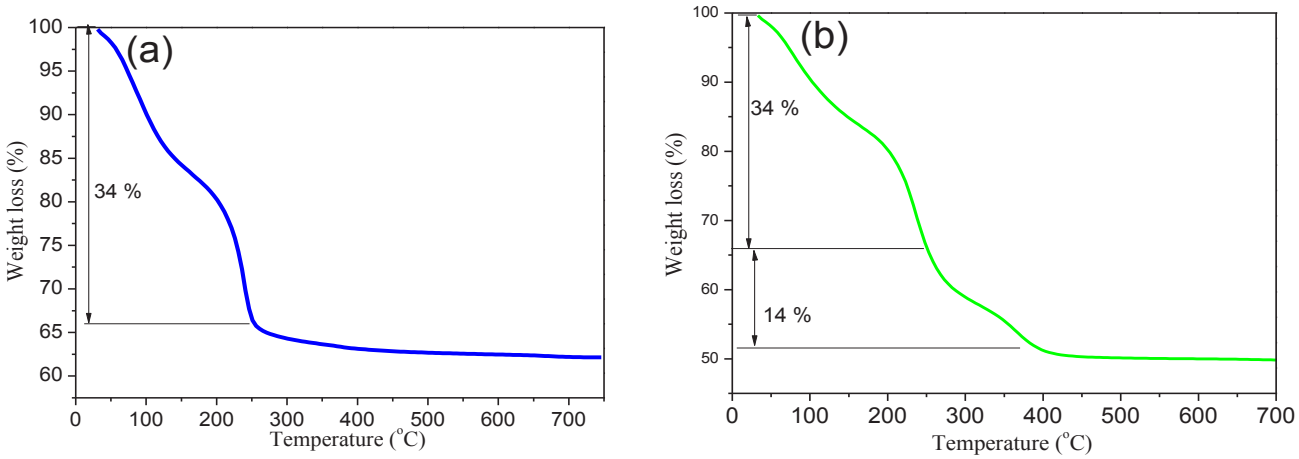

Fig. 6 Thermo gravimetric analysis of TiO_2 and SA-TiO_2 NPs (R = 0.25)

surface area (double the pure TiO_2 NPs) and pore volume. The pore sizes of the catalysts range between 8-10 nm, indicate that TiO_2 and SA-TiO_2 NPs were mesoporous. Surface area, pore size and pore volume of TiO_2 and SA-TiO_2 NPs are given in Table 1. Zhu et al. fabricated TiO_2 NPs by electro spinning method [15] and the surface area was 34 m^2/g, lower than the present work. Reddy et al. synthesised TiO_2 NPs by molten salt method [12] and the surface area was 80 m^2/g.

3.8 Evaluation of photocatalytic activity of phenol

The photocatalytic activity of pure TiO_2 and SA-TiO_2 NPs (R = 0.125, 0.25, 0.375 and 0.5) was studied by observing the degradation of phenol. From Fig. 8, it confirms that the maximum degradation of phenol was observed for SA-TiO_2 NPs (R = 0.25). The degradation process depends on the surface area of the catalyst. As the surface area increases, the number of active sites increases, hence more phenol molecules are adsorbed and degradation increases.

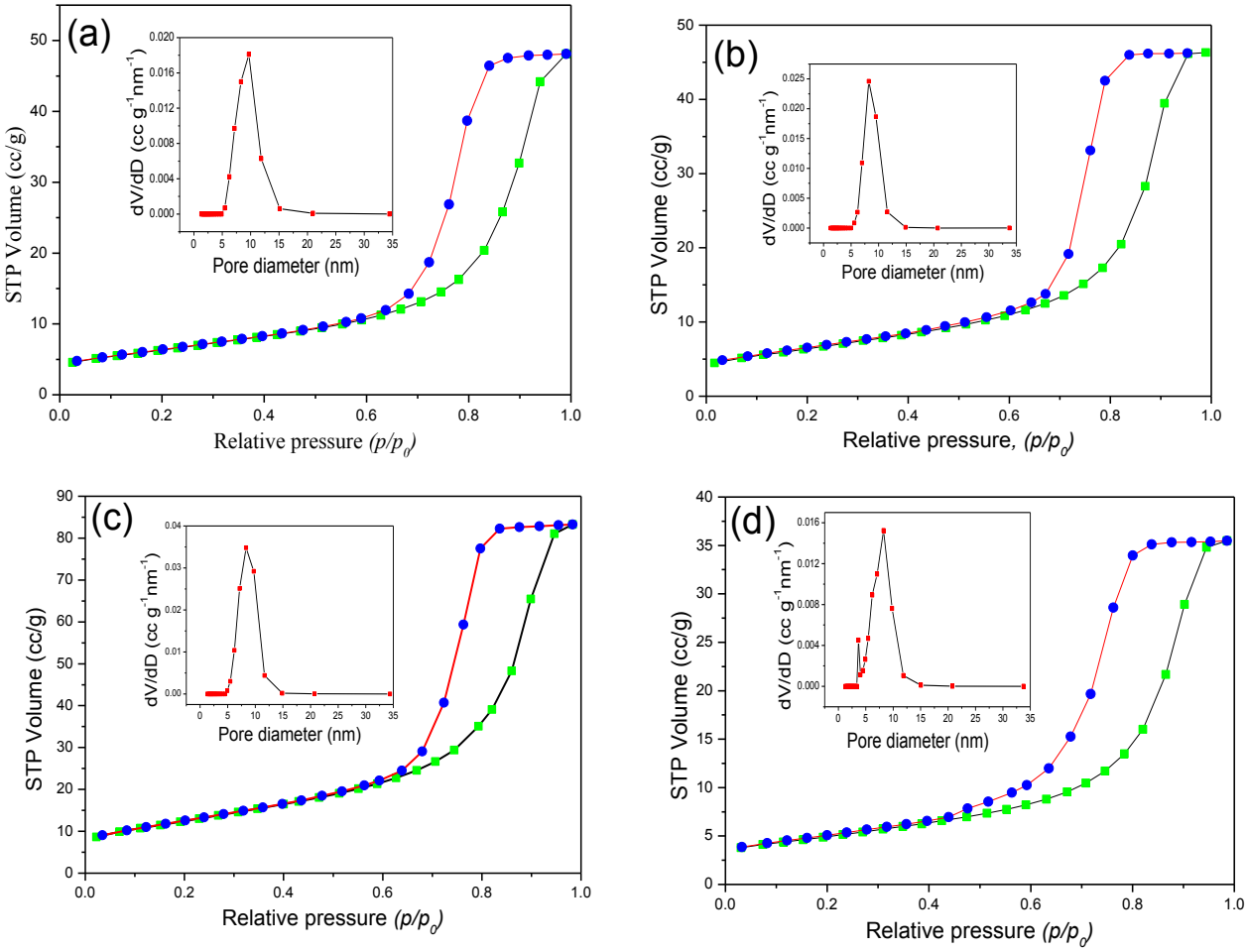

Fig. 7 N_2 physisorption isotherms and pore size distribution (inset) of (a) TiO_2 and (b, c and d) SA-TiO_2 NPs (R = 0.125, 0.25 and 0.375).

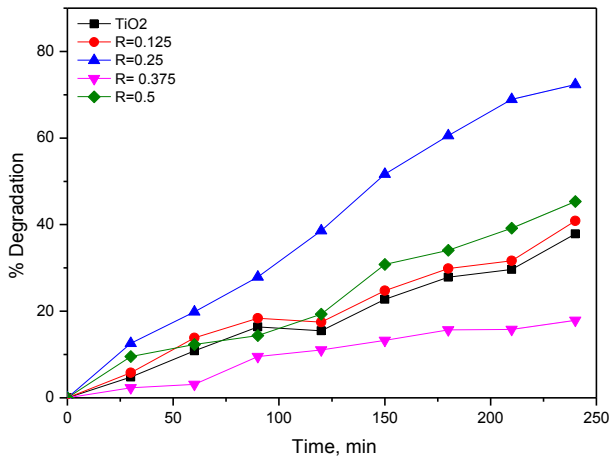

Fig. 8 Degradation of phenol using TiO_2 and SA-TiO_2 NPs at natural pH. Phenol: 0.106 mmol/L Dosage: 0.5 g/L

These results were in good agreement with the BET surface area results also i.e., the maximum specific surface area was obtained for SA-TiO_2 NPs (R = 0.25). Further, photocatalytic degradation of phenol was studied using SA-TiO_2 NPs (R = 0.25) by varying the catalyst dose and initial concentration of phenol.

3.8.1 Effect of catalyst dosage

The catalyst dosage was varied from 0.25 g/L to 1.5 g/L at a fixed phenol concentration of 0.21 mmol/L and the experimental results are presented in Fig. 9. It reveals that the phenol degradation efficiency increases with increase in catalyst concentration up to 1 g/L; while the rate decreases with further increase in catalyst concentration. The phenol degradation was maximum at 1 g/L dose of SA-TiO_2 NPs.

With increase in catalyst dose the number of active sites increases, which causes more hydroxyl radicals generation on the surface of catalyst. At higher catalyst dose above 1 g/L, the system opacity increases; causing decrease in the penetration of UV light [36]. Thus a higher dose above 1 g/L results in scattering of UV light and aggregation.

The degradation of phenol leads to the formation of intermediates such as catechol and hydroquinone. These aromatic compounds undergo oxidation to yield aldehydes

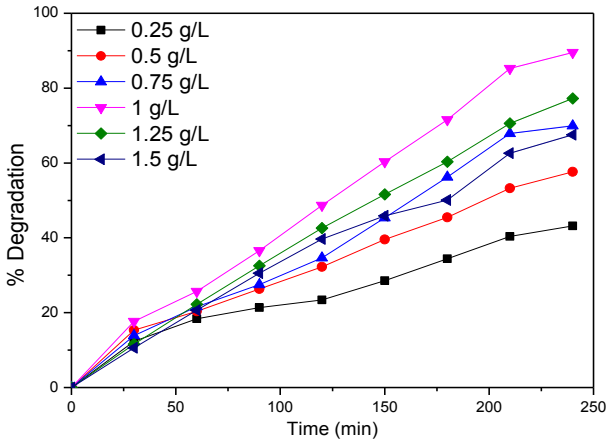

Fig. 9 Effect of SA-TiO_2 (R = 0.25) NPs on photocatalytic degradation of phenol at natural pH. Phenol: 0.21 mmol/L. Dosage: 0.25 -1.5 g/L

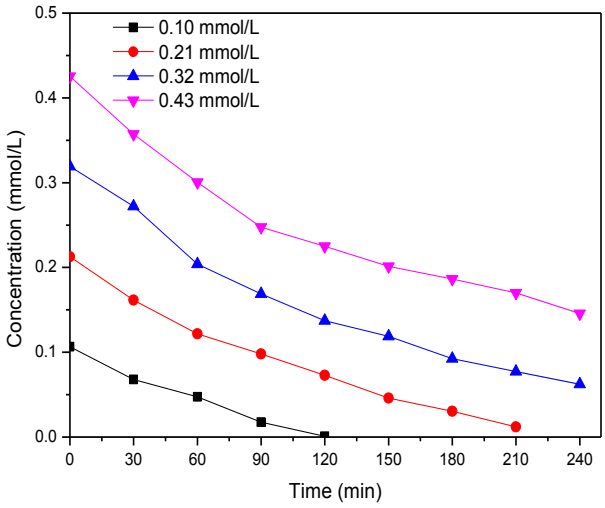

Fig. 10 Effect of phenol concentration on photocatalytic degradation of phenol at natural pH.

and carboxylic acids. De-carboxylation of these compounds lead to CO_2 and H_2O [37].

3.8.2 Effect of phenol concentration

The initial concentration of phenol was varied from 0.10 - 0.43 mmol/L (10-40 ppm) keeping the catalyst dose 1 g/L and the results are shown in Fig. 10. As the concentration of phenol increases, the degradation rate decreased. Maximum degradation rate was observed for 0.10 mmol/L phenol concentration. As the concentration of phenol increases, light absorbed by phenol is more compared to that of SA-TiO_2 NPs. The light absorbed by phenol is not available to carry out the phenol degradation. The equilibrium adsorption of phenol on active sites increases, more and more phenol molecules get adsorbed on the catalyst surface. Competitive adsorption of OH^- on the same site decreases and hence the amount of hydroxyl radicals ($OH^·$) on the catalyst surface decreases.

Hence the possibility of phenol molecules to react with $OH^·$ decreases resulting in lower degradation efficiency [38]. About 92 % of phenol was degraded within 4 h at natural pH. Phenol degradation results obtained were better compared to the earlier work [38].

3.8.3 Kinetics of photocatalytic degradation

The photocatalytic degradation of phenol follows first order kinetics as shown in the below equation

$$\ln\left(Co/C\right) = kt \tag{4}$$

where Co is the initial concentration, C is the degradation concentration after time t, k is the rate constant. The plots of ln(Co/C) vs time gave straight lines, which confirms the

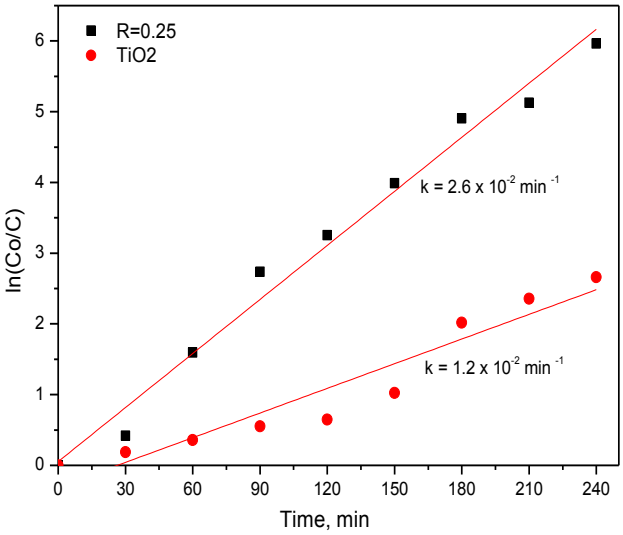

Fig. 11 Rate constants of TiO_2 and SA-TiO_2 (R = 0.25) NPs

first order degradation as shown in Fig. 11. The slopes of the straight lines are the rate constants for photocatalytic degradation of phenol for TiO_2 and SA-TiO_2 (R = 0.25) NPs.

The rate constant of SA-TiO_2 NPs was 2.6 x 10^{-2} min^{-1}, which was more than double the pure TiO_2 NPs. The rate constant obtained was higher compared to the previous literature values [38].

3.8.4 Photocatalytic degradation of salicylic acid and caffeine

The photocatalytic activity of SA-TiO_2 NPs (R = 0.25) was also measured by degradation of salicylic acid (0.145 mmol/L) and caffeine (0.103 mmol/L) under UV light source. The degradation of these pollutants was observed by the absorption of light at maximum

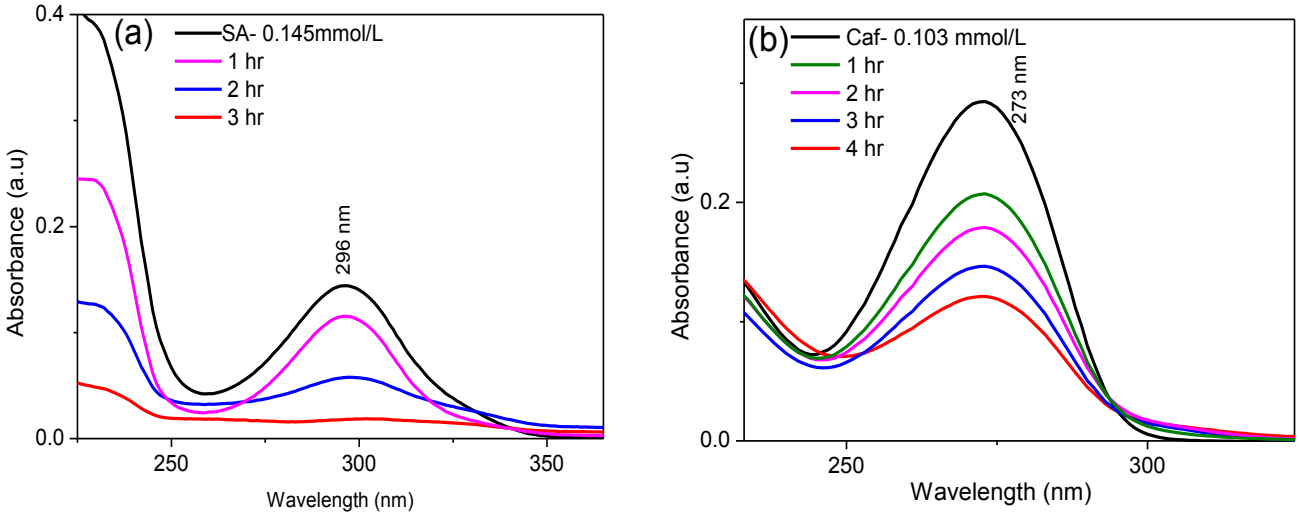

Fig. 12 (a) UV- visible absorption spectra showing the photocatalytic activity of SA-TiO_2 NPs (R = 0.25) towards photocatalytic degradation of salicylic acid at natural pH. (b) UV- visible absorption spectra showing the photocatalytic activity of SA-TiO_2 NPs (R = 0.25) towards photocatalytic degradation of caffeine at natural pH.

wavelengths, 296 nm and 273 nm for salicylic acid and caffeine respectively. The intensity of absorption peaks decreased with time as shown in Fig. 12 (a), (b). The percentage degradation of salicylic acid was 88 % in 3 h and that of caffeine was 59 % in 4 h duration.

3.8.5 Hydroxyl radical detection using coumarin as probe molecule

100 mg of SA-TiO_2 NPs was added to 50 mL of 1 mM coumarin solution. The solution was irradiated under the UV source in photo reactor. 2 mL of aliquots were withdrawn at every 10 min and the photoluminescence was measured. The coumarin (non-luminescent) reacts with hydroxyl radicals to form 7-hydroxyl coumarin (luminescent), which shows the photoluminescence peak at 454 nm. The intensity of the peak increases with irradiation time indicating the increase in concentration of hydroxyl radicals as shown in Fig. 13.

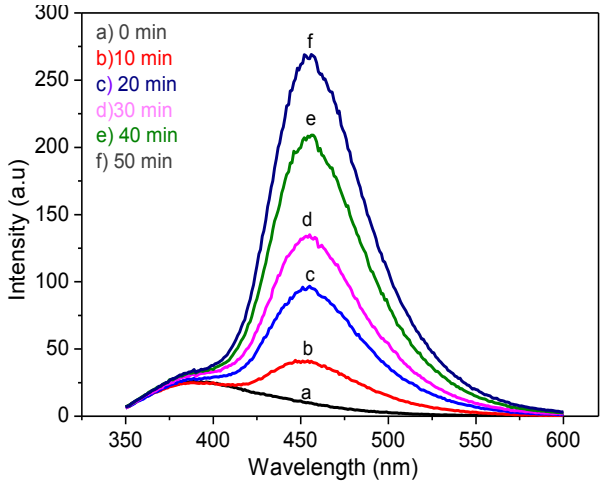

Fig. 13 Photoluminescence spectra for detection of hydroxyl radicals using coumarin as probe molecule.

4 Conclusions

TiO_2 and SA-TiO_2 NPs were successfully synthesised by modified sol-gel method. The NPs were in anatase form and mesoporous in nature. SA-TiO_2 NPs (R = 0.25) possessed a higher specific surface area and lower band gap energy compared to TiO_2 NPs. SA-TiO_2 NPs (R = 0.25) prepared using surfactant showed a higher photocatalytic activity for the degradation of phenol. The percentage degradation of phenol obtained in our work (92 %) was higher than the value reported in the literature. The rate constant for phenol degradation was found to be 2.6 x 10^{-2} min^{-1}. The percentage degradation of salicylic acid and caffeine were 88 % and 59 % respectively using SA-TiO_2 NPs (R = 0.25). The SA-TiO_2 NPs can be an effective photocatalyst for the removal of organic contaminants from the industrial waste water under UV light irradiation.

Acknowledgement

One of the authors Dr. Nagaraju would like to acknowledge DST Nanomission, Govt. of India, New Delhi (Project No. SR/NM/NS-1262/2013) for the financial support to carry out this research work. Authors would like to thank COE – TEQIP -2, Director and Principal, SIT, Tumakuru for constant support and encouragement of the research activities.

References

[1] Chatterjee, D., Dasgupta, S. "Visible light induced photocatalytic degradation of organic pollutants", Journal of Photochemistry and Photobiology C: Photochemistry Reviews, 6(2–3), pp. 186–205, 2005. https://doi.org/10.1016/j.jphotochemrev.2005.09.001

[2] Murcia-López, S., Hidalgo, M. C., Navío, J. A. "Synthesis, characterization and photocatalytic activity of Bi-doped TiO_2 photocatalysts under simulated solar irradiation", Applied Catalysis A: General, 404(1–2), pp. 59–67, 2011. https://doi.org/10.1016/j.apcata.2011.07.008

[3] Mali, S. S., Shinde, P. S., Betty, C. A., Bhosale, P. N., Lee, W. J., Patil, P. S. "Nanocoral architecture of TiO_2 by hydrothermal process: Synthesis and characterization", Applied Surface Science, 257(23), pp. 9737–9746, 2011. https://doi.org/10.1016/j.apsusc.2011.05.119

[4] Lu, C.-H., Wen, M.-C. "Synthesis of nanosized TiO_2 powders via a hydrothermal microemulsion process", Journal of Alloys and Compounds, 448(1–2), pp. 153–158, 2008. https://doi.org/10.1016/j.jallcom.2007.01.043

[5] Li, H., Cao, L., Liu, W., Su, G., Dong, B. "Synthesis and investigation of TiO_2 nanotube arrays prepared by anodization and their photocatalytic activity", Ceramics International, 38(7), pp. 5791–5797, 2012. https://doi.org/10.1016/j.ceramint.2012.04.026

[6] Ito, A., Sato, T., Goto, T. "Transparent anatase and rutile TiO_2 films grown by laser chemical vapor deposition", Thin Solid Films, 551, pp. 37–41, 2014. https://doi.org/10.1016/j.tsf.2013.11.089

[7] Akhavan Sadr, F., Montazer, M. "In situ sonosynthesis of nano TiO_2 on cotton fabric", Ultrasonics Sonochemistry, 21(2), pp. 681–691, 2014. https://doi.org/10.1016/j.ultsonch.2013.09.018

[8] Suprabha, T., Roy, H. G., Thomas, J., Praveen Kumar, K., Mathew, S. "Microwave-Assisted Synthesis of Titania Nanocubes, Nanospheres and Nanorods for Photocatalytic Dye Degradation", Nanoscale Research Letters, 4(2), pp. 144–152, 2009. https://doi.org/10.1007/s11671-008-9214-5

[9] Musić, S., Gotić, M., Ivanda, M., Popović, S., Turković, A., Trojko, R., Sekulić, A., Furić, K. "Chemical and micro structural properties of TiO_2 synthesized by sol-gel procedure", Materials Science and Engineering: B, 47(1), pp. 33–40, 1997. https://doi.org/10.1016/S0921-5107(96)02041-7

[10] Reddy, M. V, Rao, G. V. S., Chowdari, B. V. R. "Metal Oxides and Oxysalts as Anode Materials for Li Ion Batteries", Chemical Reviews, 113(7), pp. 5364-5457, 2013. https://doi.org/10.1021/cr3001884

[11] Reddy, M. V, Jose, R., Teng, T. H., Chowdari, B. V. R., Ramakrishna, S. "Electrochimica Acta Preparation and electrochemical studies of electrospun TiO_2 nanofibers and molten salt method nanoparticles", Electrochimica Acta, 55(9), pp. 3109–3117, 2010. https://doi.org/10.1016/j.electacta.2009.12.095

[12] Reddy, M. V, Teoh, X. W. V., Nguyen, T. B., Lim, Y. Y. M., Chowdari, B. V. R. "Effect of 0.5 M $NaNO_3$: 0.5 M KNO_3 and 0.88 M $LiNO_3$: 0.12 M LiCl Molten Salts, and Heat Treatment on Electrochemical Properties of TiO_2", Journal of The Electrochemical Society, 159(6), pp. 762–769, 2012. https://doi.org/10.1149/2.077206jes

[13] Reddy, M. V, Sharma, N., Adams, S., Rao, R. P., Peterson, V. K., Chowdari, B. V. R. "Evaulation of undoped and M-doped TiO_2, where M = Sn, Fe, Ni/Nb, Zr, V, and Mn, for lithium-ion battery applications prepared by the molten-salt method", RSC Advances, 5, pp. 29535–29544, 2015. https://doi.org/10.1039/C5RA00206K

[14] Reddy, M. V, Adams, S., Liang, G. T. J., Mingze, I. F., An, H. V. T., Chowdari, B. V. R. "Low temperature molten salt synthesis of anatase TiO_2 and its electrochemical properties", Solid State Ionics, 262, pp. 120–123, 2013. https://doi.org/10.1016/j.ssi.2013.11.030

[15] Zhu, P., Wu, Y., Reddy, M. V., Nair, A. S., Chowdari, B. V. R., Ramakrishna, S. "Long term cycling studies of electrospun TiO_2 nanostructures and their composites with MWCNTs for rechargeable Li-ion batteries", RSC Advances, 2, pp. 531–537, 2012. https://doi.org/10.1039/c1ra00514f

[16] Cherian, C. T., Reddy, M. V., Magdaleno, T., Sow, C.-H., Ramanujachary, K. V., Rao, G. V. S., Chowdari, B. V. R. "(N, F) - Co - doped TiO_2: synthesis, anatase - rutile conversion and Li - cycling properties." CrystEngComm, 14, pp. 978–986, 2012. https://doi.org/10.1039/c1ce05685a

[17] Zhang, Q., Gao, L., Guo, J. "Effect of hydrolysis conditions on morphology and crystallization of nanosized TiO_2 powder", Journal of the European Ceramic Society, 20(12), pp. 2153–2158, 2000. https://doi.org/10.1016/S0955-2219(00)00085-6

[18] Wang, J., Li, S., Yan, W., Tse, S. D., Yao, Q. "Synthesis of TiO_2 nanoparticles by premixed stagnation swirl flames", Proceedings of the Combustion Institute, 33(2), pp. 1925–1932, 2011. https://doi.org/10.1016/j.proci.2010.05.022

[19] Li, G. L., Wang, G. H. "Synthesis of nanometer-sized TiO_2 particles by a microemulsion method", Nanostructured Materials, 11(5), pp. 663–668, 1999. https://doi.org/10.1016/S0965-9773(99)00354-2

[20] Macwan, D. P., Dave, P. N., Chaturvedi, S. "A review on nano-TiO_2 sol–gel type syntheses and its applications", Journal of Materials Science, 46(11), pp. 3669–3686, 2011. https://doi.org/10.1007/s10853-011-5378-y

[21] Hoffmann, M. R., Martin, S. T., Choi, W., Bahnemannt, D. W. "Environmental Applications of Semiconductor Photocatalysis", Chemical Reviews, 95(1), pp. 69–96, 1995. https://doi.org/10.1021/cr00033a004

[22] Dholam, R., Patel, N., Adami, M., Miotello, A. "Hydrogen production by photocatalytic water-splitting using Cr- or Fe-doped TiO_2 composite thin films photocatalyst", International Journal of Hydrogen Energy, 34(13), pp. 5337–5346, 2009. https://doi.org/10.1016/j.ijhydene.2009.05.011

[23] Feng, H., Zhang, M.-H., Yu, L. E. "Hydrothermal synthesis and photocatalytic performance of metal-ions doped TiO_2", Applied Catalysis A: General, 413–414, pp. 238–244, 2012. https://doi.org/10.1016/j.apcata.2011.11.014

[24] Yu, J., Xiong, J., Cheng, B., Liu, S. "Fabrication and characterization of Ag-TiO_2 multiphase nanocomposite thin films with enhanced photocatalytic activity", Applied Catalysis B: Environmental, 60(3–4), pp. 211–221, 2005. https://doi.org/10.1016/j.apcatb.2005.03.009

[25] Han, C., Andersen, J., Likodimos, V., Falaras, P., Linkugel, J., Dionysiou, D. D. "The effect of solvent in the sol-gel synthesis of visible light-activated, sulfur-doped TiO_2 nanostructured porous films for water treatment", Catalysis Today, 224, pp. 132–139, 2014. https://doi.org/10.1016/j.cattod.2013.11.052

[26] Jun, Y., Casula, M. F., Sim, J.-H., Kim, S. Y., Cheon, J., Alivisatos, A. P. "Surfactant-Assisted Elimination of a High Energy Facet as a Means of Controlling the Shapes of TiO_2 Nanocrystals", Journal of the American Chemical Society, 125(51), pp. 15981–15985, 2003. https://doi.org/10.1021/ja0369515

[27] Dionysiou, D. D., Khodadoust, A. P., Kern, A. M., Suidan, M. T., Baudin, I., Laîné, J.-M. "Continuous-mode photocatalytic degradationof chlorinated phenols and pesticides in water using a bench-scale TiO_2 rotating disk reactor", Applied Catalysis B: Environmental, 24(3-4), pp. 139–155, 2000. https://doi.org/10.1016/S0926-3373(99)00103-4

[28] Ozyonar, F., Aksoy, S. "Removal of Salicylic Acid from Aqueous Solutions Using Various Electrodes and Different Connection Modes by Electrocoagulation", International Journal of Electrochemical Science, 11, pp. 3680–3696, 2016. https://doi.org/10.20964/110454

[29] Halling-Sørensen, B., Nielsen, S. N., Lanzky, P. F., Ingerslev, F., Lützhøft, H. C. H., Jørgensen, S. E. "Occurrence, fate and effects of pharmaceutical substnaces in the environment - A review", Chemosphere, 36(2), pp. 357–393, 1998. https://doi.org/10.1016/S0045-6535(97)00354-8

[30] Chuang, L. C., Luo, C. H., Huang, S. W., Wu, Y. C., Huang, Y. C. "Photocatalytic Degradation Mechanism and Kinetics of Caffeine in Aqueous Suspension of Nano-TiO_2", Advanced Materials Research, 214, pp. 97–102, 2011. https://doi.org/10.4028/www.scientific.net/AMR.214.97

[31] Arfanis, M. K., Adamou, P., Moustakas, N. G., Triantis, T. M., Kontos, A. G., Falaras, P. "Photocatalytic degradation of salicylic acid and caffeine emerging contaminants using titania nanotubes." Chemical Engineering Journal, 310(2), pp. 525–536, 2017. https://doi.org/10.1016/j.cej.2016.06.098

[32] Zhang, W., Liu, Y., Pei, X., Chen, X. "Effects of indium doping on properties of xIn-0.1%Gd-TiO_2 photocatalyst synthesized by sol-gel method", Journal of Physics and Chemistry of Solids, 104, pp. 45–51, 2017. https://doi.org/10.1016/j.jpcs.2016.12.031

[33] Beydoun, D., Amal, R. "Implications of heat treatment on the properties of a magnetic iron oxide-titanium dioxide photocatalyst", Materials Science and Engineering: B, 94(1), pp. 71–81, 2002. https://doi.org/10.1016/S0921-5107(02)00085-5

[34] Liao, D. L., Liao, B. Q. "Shape , size and photocatalytic activity control of TiO_2 nanoparticles with surfactants", Journal of Photochemistry and Photobiology A: Chemistry, 187(2-3), pp. 363–369, 2007. https://doi.org/10.1016/j.jphotochem.2006.11.003

[35] Murphy, A. B. "Band-gap determination from diffuse reflectance measurements of semiconductor films, and application to photoelectrochemical water-splitting", Solar Energy Materials and Solar Cells, 91(14), pp. 1326–1337, 2007. https://doi.org/10.1016/j.solmat.2007.05.005

[36] Amalraj, A. "Photocatalytic Degradation of Alizarin Red S and Bismarck Brown R Using TiO 2 Photocatalyst", (September). 2015.

[37] Nagaveni, K., Sivalingam, G., Hegde, M. S., Madras, G. "Photocatalytic Degradation of Organic Compounds over Combustion-Synthesized Nano-TiO_2", Environmental Science & Technology, 38(5), pp. 1600–1604, 2004. https://doi.org/10.1021/es034696i

[38] Naeem, K., Feng, O. "Parameters effect on heterogeneous photocatalysed degradation of phenol in aqueous dispersion of TiO_2", Journal of Environmental Sciences, 21(4), pp. 527–533, 2009. https://doi.org/10.1016/S1001-0742(08)62303-7